Catalysis Today 433 (2024) 114667

Contents lists available at ScienceDirect

Catalysis Today

journal homepage: www.elsevier.com/locate/cattod

Biogas upgrading by intensified methanation (SESaR): Reaction plus water adsorption - desorption cycles with Ni-Fe/Al_2O_3 catalyst and LTA 5A zeolite

Víctor Daniel Mercader, Paúl Durán, Pablo Aragüés-Aldea, Eva Francés, Javier Herguido, José Angel Peña *

Catalysis and Reactor Engineering Group (CREG), Aragon Institute of Engineering Research (I3A), Universidad Zaragoza, 50.018, Zaragoza, Spain

ARTICLE INFO

Keywords:
Biogas
Biomethane
Hydrogenation
Renewable hydrogen
Synthetic natural gas

ABSTRACT

This work is conducted within the framework of the *Power to Gas* (*PtG*) technologies, focusing on the topic of "*biogas upgrading*". The objective is to enhance the CH_4 content of biogas streams by utilizing the CO_2 present in these streams through the *Sabatier* reaction, thereby producing a renewable alternative to natural (*fossil*) gas. Referred to as "*SESaR*"(*Sorption Enhanced Sabatier Reaction*), this process employs a catalytic fixed-bed reactor, featuring selective water adsorption using LTA 5A zeolites, as an innovative approach to traditional methanation reactors. The catalyst used comprises Ni-Fe (7.5:2.5 $^{wt}/_{wt}$) as the active metallic phase supported on γ-Al_2O_3. Experimental work has been divided in two sets of trials. The first set focuses on the hydrogenation of CO_2 as single reactant (H_2 also supplied in the inlet with 4:1 = H_2:CO_2 molar ratio). The second set of experiments was carried out with a synthetic gas mixture representative of a sweetened biogas stream (molar ratio CH_4:CO_2 = 7:3). Maximum intensification behavior for CO_2 conversion was found at 350 °C, also showing that CH_4 presence in the inlet gas has negligible influence on the conversion of CO_2. Selectivity to CO is minimized at temperatures exceeding 300 °C and remains constant after three consecutive cycles of methanation, water adsorption, and desorption. The Fe-Ni catalyst has demonstrated sustained performance throughout the experimental cycles, exhibiting no significant loss of activity.

1. Introduction

Society is nowadays facing important challenges, such as reducing carbon emissions or ensuring the capacity of covering increasing energy demands in a sustainable way. Even if some of these goals could be apparently solved by implementing new renewable energy sources, questions about how to store the temporary surpluses of renewable electricity, or ensure a stable energy provision, are still unanswered. Moreover, in last years the European energy mix has been questioned because of its huge dependency on international providers for satisfying the inner energy demand (mainly oil and natural gas) [1,2]. Even though global interests and research efforts have been put on hydrogen production as energy vector, important questions such as its transport, storage and normative remain non answered. A pool of alternative energy vectors can facilitate the energy transition, being especially interesting those with relatively high energy density such as ammonia [3], methanol [4] or methane [5].

Power to Gas (PtG or P2G) technologies have been proposed by several authors as a feasible alternative for methanation processes [6,7]. In the case described in this work, PtG objective consists in producing methane from renewable H_2 generated by water electrolysis and highly concentrated streams of CO_2. For such purpose, energy should be supplied by surplus electricity from renewables (i.e. wind, tidal or solar) [8]. The CO_2, on the other side, could be sequestrated from highly concentrated streams such as biogas (ca. 40%^{v} CO_2 + 60%^{v} CH_4) or other sources like biomass or sewage sludge gasification streams [9,10]. *Sabatier* reaction (r.1) produces methane and water [11] with the aid of a catalyst. However, methanation process mechanism can also be considered the combination of the *Reverse Water-Gas Shift* reaction (rWGS) (r.2) [12], followed by the hydrogenation of CO (*Reverse Steam Methane Reforming* -rSMR-) [13]. If CO_2 contained in a biogas is used as raw material for methanation, the upgraded biogas could achieve a concentration in methane higher than 95%^{v}, giving rise to a so called *Synthetic Natural Gas* [14], provided that other requirements are fulfilled like an appropriate *Wobbe* number, or a maximum content in H_2S, CO and CO_2. Thus, PtG technologies can produce an energy vector easier

* Corresponding author.
E-mail address: jap@unizar.es (J.A. Peña).

https://doi.org/10.1016/j.cattod.2024.114667
Received 20 December 2023; Received in revised form 12 February 2024; Accepted 22 March 2024
Available online 25 March 2024

(*cheaper*) to transport and store than hydrogen. In fact, the technology required to adapt the preexisting natural gas network to synthetic natural gas is quite simple, being and interesting substitute of fossil natural gas [15].

$$CO_2 + 4H_2 \rightleftharpoons CH_4 + 2H_2O \quad \Delta H_r^0 = -165.1[kJ\cdot mol^{-1}] \tag{r.1}$$

$$CO_2 + H_2 \rightleftharpoons CO + H_2O \quad \Delta H_r^0 = +41.2[kJ\cdot mol^{-1}] \tag{r.2}$$

$$CO + 3H_2 \rightleftharpoons CH_4 + H_2O \quad \Delta H_r^0 = -206.3[kJ\cdot mol^{-1}] \tag{r.3}$$

Several catalysts have been reported in bibliography to improve the conversion of CO_2 and H_2 to methane (r.1), being ruthenium and nickel among the most common because of their selectivity and activity [16]. Nevertheless, both catalysts show important limitations for their scale up in industrial practice [17]. On the one hand, the limiting factor for Ru is its high price and availability; on the other, higher Ni loads are needed to achieve similar conversions than those of Ru. In addition, undesired carbonaceous residues (coke) tend to appear for Ni based catalysts [18]. Other noteworthy catalysts, based on nickel with various supports like ceria or others, have been described in recent literature [19–22].

A possible solution for overcoming these limitations is to combine the effect of two metals as active species in one catalyst. Fe and Ni blended in adequate proportions produce similar yields towards CH_4 than Ru catalysts, while its total cost decreases and the coking behavior can be kept under control [23].

From the thermodynamical point of view, an intensification of conventional methanation processes is the so-called *Sorption Enhanced Sabatier Reactor* (SESaR). SESaR technology includes a water adsorbent present in the catalytic bed, which can push up the conversion of reactants, even beyond the limits predicted by equilibrium, by continuous removing of one of the species (H_2O) formed in reactions ((r.1) to (r.3)), as it is prescribed by *Le Châtelier's* principle.

In this work a fixed bed reactor was loaded with a lab-made Ni-Fe based catalyst supported on γ-Al_2O_3 and an LTA zeolite 5A as water adsorbent. The selection of the catalyst was based on the positive results of previous studies [24]. In these, a Ni-Fe catalyst (7.5:2.5 ^{wt}% over 90 ^{wt}% γ-Al_2O_3) showed conversion and selectivity values close to Ru catalyst at comparable reaction conditions.

2. Experimental

2.1. Solids and characterization

The catalyst (7.5%^{wt} Ni and 2.5%^{wt} Fe, labelled as 7.5Ni-2.5Fe) was synthesized by incipient wetness impregnation from $Ni(NO_3)_2{\cdot}6\ H_2O$ and $Fe(NO_3){\cdot}9\ H_2O$, both from *Sigma Aldrich*. In addition, a commercial γ-Al_2O_3 (ca. 200 m^2/g, *Puralox, SASOL*) was selected as support material for the catalyst. After impregnation, the catalyst was dried at 65 °C for 16 hours and then at 90 °C for 8 hours. Afterward, the dried catalyst was calcined (B180, *Nabertherm*) in air at 500 °C for 8 hours (β= 5 °C/min). The catalyst was then crushed and sieved. Finally, it was activated at 500 °C for 2 hours with a gas flow composed of 50%^{v} H_2, 45%^{v} Ar and 5%^{v} N_2 immediately prior to its use in the reactor. Zeolite LTA 5A was purchased from *Alfa Aesar* as water adsorbent. Following the same procedure used with catalyst, zeolite was sieved to the desired particle size.

Several characterization techniques were applied to the solids, including N_2 adsorption-desorption isotherms (BET), X-ray fluorescence for composition (XRF) and X-ray diffraction (XRD) for the identification of crystalline structures in the catalyst and the zeolite. Temperature programmed reduction (TPR) (β= 5 °C/min) was only used for the catalyst with a H_2/N_2 flow of 100 mL(STP)/min and hydrogen partial pressure of 0.05 bar out of 1 bar of total pressure. Results of TPR (not shown, but available in [24]) demonstrate that the addition of Fe produced a decrease in the reduction temperature of the Ni/Fe alloy.

Table 1
Surface area of the solids (BET).

Solid	BET area ($m^2{\cdot}g^{-1}$)
γ-Al_2O_3 fresh	200.6 ± 0.4
10Ni	174.5 ± 0.3
7.5Ni-2.5Fe	167.4 ± 0.4
Zeolite 5A	428.1 ± 8.0

Table 2
Chemical composition of the solids measured by XRF. Nominal composition for 10Ni: 10 ^{w}% Ni; for 7.5Ni-2.5Fe: 7.5 ^{w}% Ni and 2.5 ^{w}% Fe; both on γ-Alumina.

Solid	Presence of element (%^{wt})					
	Ni	Fe	Si	Al	Ca	Na
10Ni	11.07 ± 0.14 0.1	-	-	45.25 ± 0.09	-	-
7.5Ni-2.5Fe	7.42 ± 0.12	2.13 ± 0.06	-	46.86 ± 0.25	-	-
Zeolite 5A	-	-	21.07 ± 0.16	19.37 ± 0.16	7.07 ± 0.11	3.28 ± 0.08

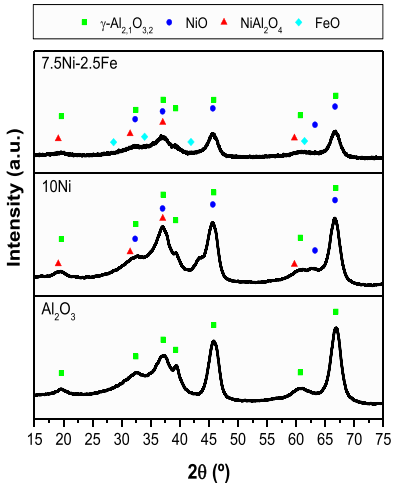

Fig. 1. XRD spectra for comparison between the two catalysts (10Ni, 7.5Ni-2.5Fe) and fresh support (γ-Al_2O_3). Colored symbols represent characteristic patterns of pure substances.

The effect of diffusional constraints (internal and external) was also studied, fixing a minimum (constant) volumetric flowrate of 250 mL (STP)·min^{-1}, and a particle size between 100 and 200 μm (for both catalyst and zeolite). Both aspects ensured kinetic regime.

BET results (Table 1) shows that the impregnation of metals on the surface and later calcination of the catalyst, provoke a decrease in the surface area respecting the fresh γ-Al_2O_3. Surface area for 7.5Ni-2.5Fe catalyst was compared with a reference 10%^{wt} of Ni catalyst (labelled as 10Ni) in order to study the effect of including a second metal in the synthesis. That comparison demonstrated a slight reduction in the BET area by adding the second metal (i.e., Fe) in the impregnation step. XRF characterization (Table 2), showed element content percentages confirming the adequate addition of precursors during the catalyst synthesis.

XRD characterization (Fig. 1) was selected as complementary technique for crystalline identification. Gamma alumina phase (γ-$Al_{2.1}O_{3.2}$) is observed in both catalysts (7.5Ni-2.5Fe and 10Ni, both on γ-Al_2O_3) and the fresh alumina sample (γ-Al_2O_3). Clearly, the presence of gamma alumina phase complicates the recognition of nickel and iron oxides, but XRD spectra point out the presence of NiO and FeO although clearly in a lower extent compared to that coming from alumina alone.

The elemental chemical analysis of the catalyst particles, conducted

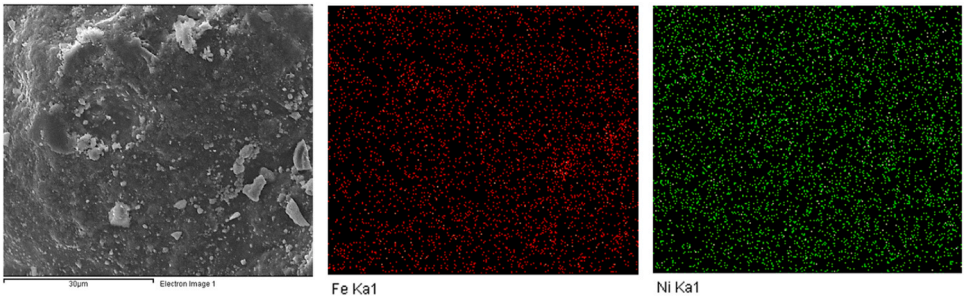

Fig. 2. *SEM image (left) for a particle of 7.5Ni+2.5Fe over γ-Al_2O_3 and EDX spectroscopy analysis showing the dispersion of iron (center -red-) and nickel (right -green-).*

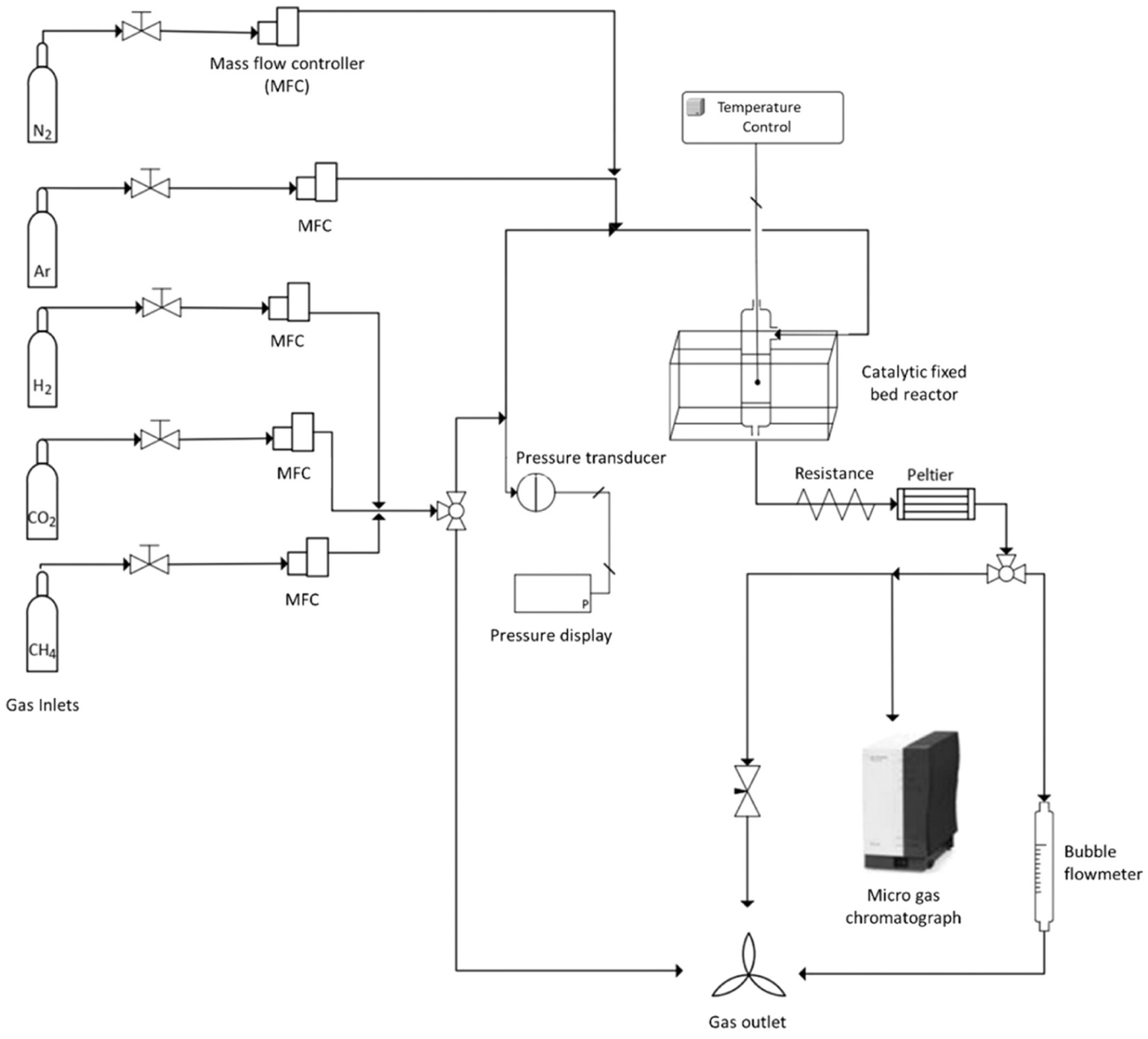

Fig. 3. Flowsheet diagram of the experimental set-up.

via Energy-dispersive X-ray spectroscopy (EDX) using an *Inspect F-50 SEM* instrument, is depicted in Fig. 2. Images show a uniform distribution of Ni (green) and Fe (red) active sites across the catalyst surface. Moreover, the elemental quantification results obtained from this technique (not shown), align with the elemental presence observed in the XRF characterization (Table 2).

2.2. Reaction setup and methodology

The experimental set-up (see Fig. 3) included a fixed bed reactor,

Table 3
Operating conditions used in the experiments.

Variable	Values
Catalyst load	0.25 g
Zeolite (LTA 5A) load	10.25 g
Particle diameter	100–200 μm
Bed height	12 cm
Reactor inner diameter	13 mm
Temperature	250, 275, 300, 325, 350, 375 and 400 °C
Volumetric flow	250 mL(STP)·min^{-1}
H_2:CO_2 molar ratio	2:1, 3:1, 4:1, 5:1 and 6:1
CH_4:CO_2 ratio (synth. biogas)	7:3
Pressure	1 atm
Thermocouple height (from supporting plate)	1, 3, 6, 9 and 12 cm

operating at atmospheric pressure (quartz, ϕ_{in}= 13 mm). The mass of solids introduced in the bed was 0.25 g of catalyst and 10.25 g of LTA 5A zeolite. Prior to starting a methanation experiment, the catalyst was activated at 500 °C for 2 hours, with a gas flow of 150 mL(STP)·min^{-1} and composition of 50%^{v} H_2, 45%^{v} Ar and 5%^{v} N_2. After the activation stage, the temperature was decreased to the experimental conditions. Methanation of CO_2 experiments were performed in the range between 450 and 250 °C (in decreasing steps ΔT of −25 or −50 °C). Total volumetric flow of 250 mL(STP)·min^{-1} and different molar ratios H_2:CO_2 (2:1, 3:1, 4:1, 5:1 and 6:1), diluted in 5%^{v} of Ar and 5%^{v} of N_2 (internal standard) were used.

On the other hand, for the methanation of synthetic biogas (CO_2 + CH_4 mixtures), the feed included a CH_4:CO_2 molar ratio of 7:3, simulating a sweetened biogas resulting from the anaerobic decomposition of MSW landfill, and H_2:CO_2 = 4:1, diluted with a 5%^{v} of Ar and 5%^{v} of N_2 (also as internal standard). Temperature control was ensured by measuring the temperature inside the reactor at five different bed lengths with the aid of 5 thermocouples in axial position at 1, 3, 6, 9 and 12 cm, measured from the support plate (vertical reactor). Table 3 summarizes the operating conditions for the methanation experiments.

The reactor was fed with a premixed reactants gas flow with the previously mentioned molar ratios through five mass flow meter and controllers (*Alicat*). The reactor configuration consisted in a fixed bed fed from the top. The catalyst bed was supported on a quartz plate gas distributor. Exhaust gases coming out from the reactor were conducted to a cold trap (*Peltier* module) where water was condensed and removed from the gas stream to prevent malfunction of the analysis system. Finally, they were led to a micro gas chromatograph (μGC) (*Agilent 490*) where their compositions were monitored.

The reactor was heated up allowing a flow mixture of argon and nitrogen up to the set-point temperature. Control thermocouple was located at a height of 6 cm from the distribution plate, in a central height axial position.

Two kinds of experiments were conducted in this work. Those used as reference of the kinetic behavior of the catalyst without the water adsorbing capacity provided by zeolites, and those which also included in their formulation, not only the catalytic activity provided by the catalyst, but also the capacity to retain adsorbed water. In such cases, after a methanation step, a desorption stage should also be included to remove the water and allow the catalyst to be prepared for the following methanation. These types of experiments were carried out both, for the hydrogenation of single CO_2, and mixtures of CO_2 with CH_4 simulating a previously sweetened biogas.

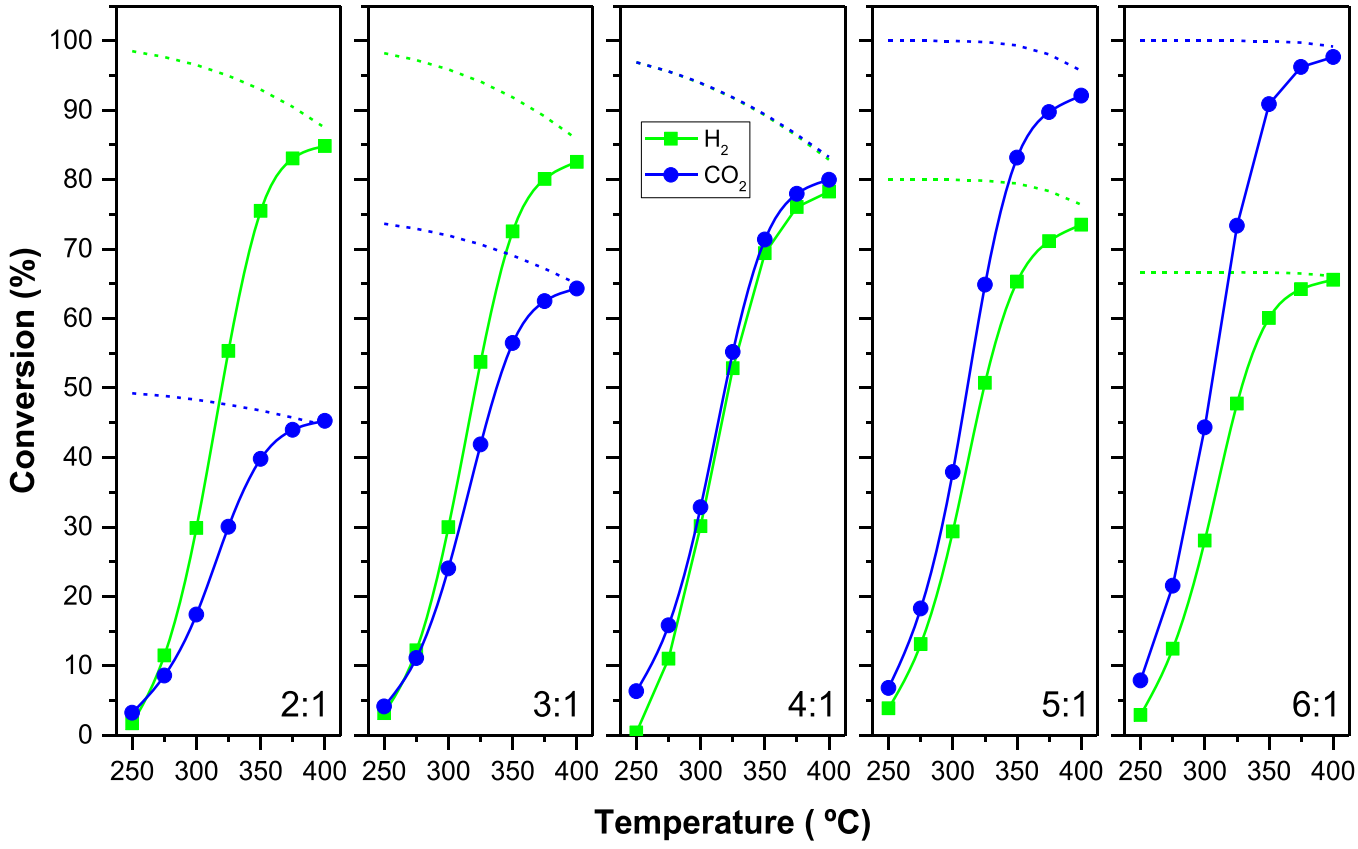

Fig. 4. H_2 and CO_2 conversion vs. temperature for different H_2:CO_2 molar ratios. Green symbols for H_2 and blue ones for CO_2. Dashed lines represent thermodynamic equilibrium conversions (green for H_2, blue for CO_2) calculated by ΔG minimization. Mass of catalyst = 0.50 g; flowrates and composition as in Table 3.

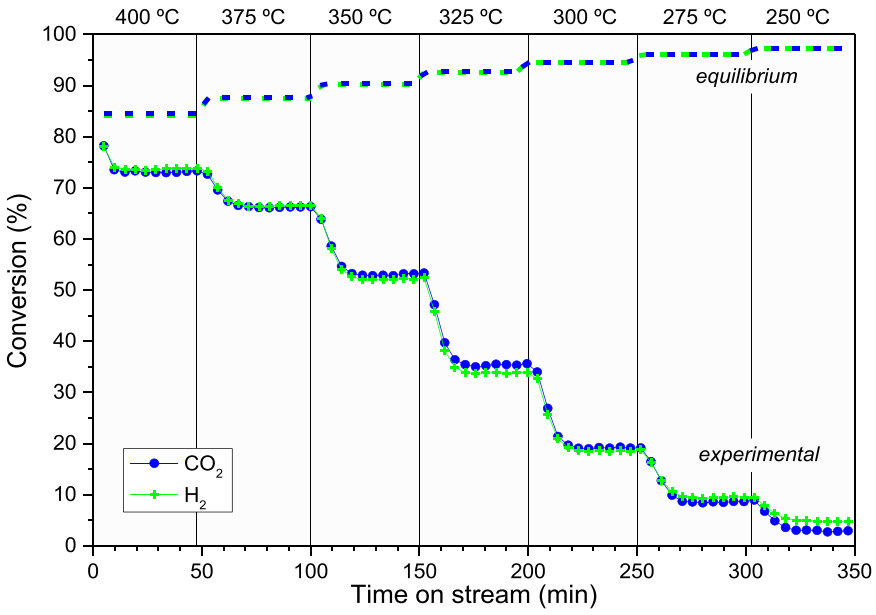

Fig. 5. CO_2 and H_2 conversions (symbols) at different temperatures for 7.5Ni-2.5Fe/γ-Al_2O_3 catalyst along methanation experiments with H_2:CO_2 ratio of 4:1. Rest of variables with standard values (see Table 3). Dashed lines denote theoretical values for equilibrium.

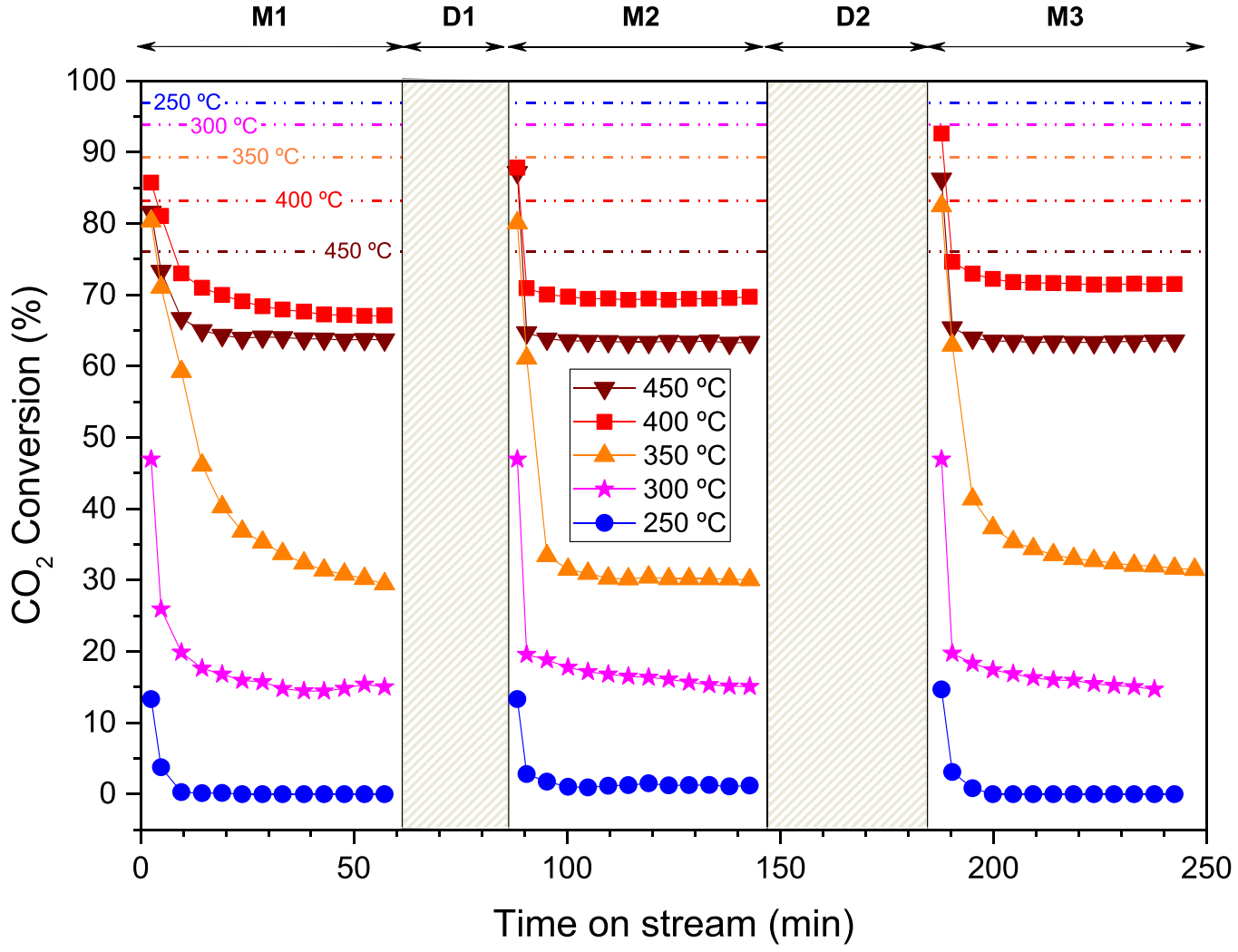

Fig. 6. CO_2 conversion for methanation-desorption experiment cycles. Feeding molar ratio H_2:CO_2 = 4:1, rest of operating conditions as in Table 3. Dashed dotted lines represent equilibrium conversions at different temperatures. Curves between data symbols only for visual guidance.

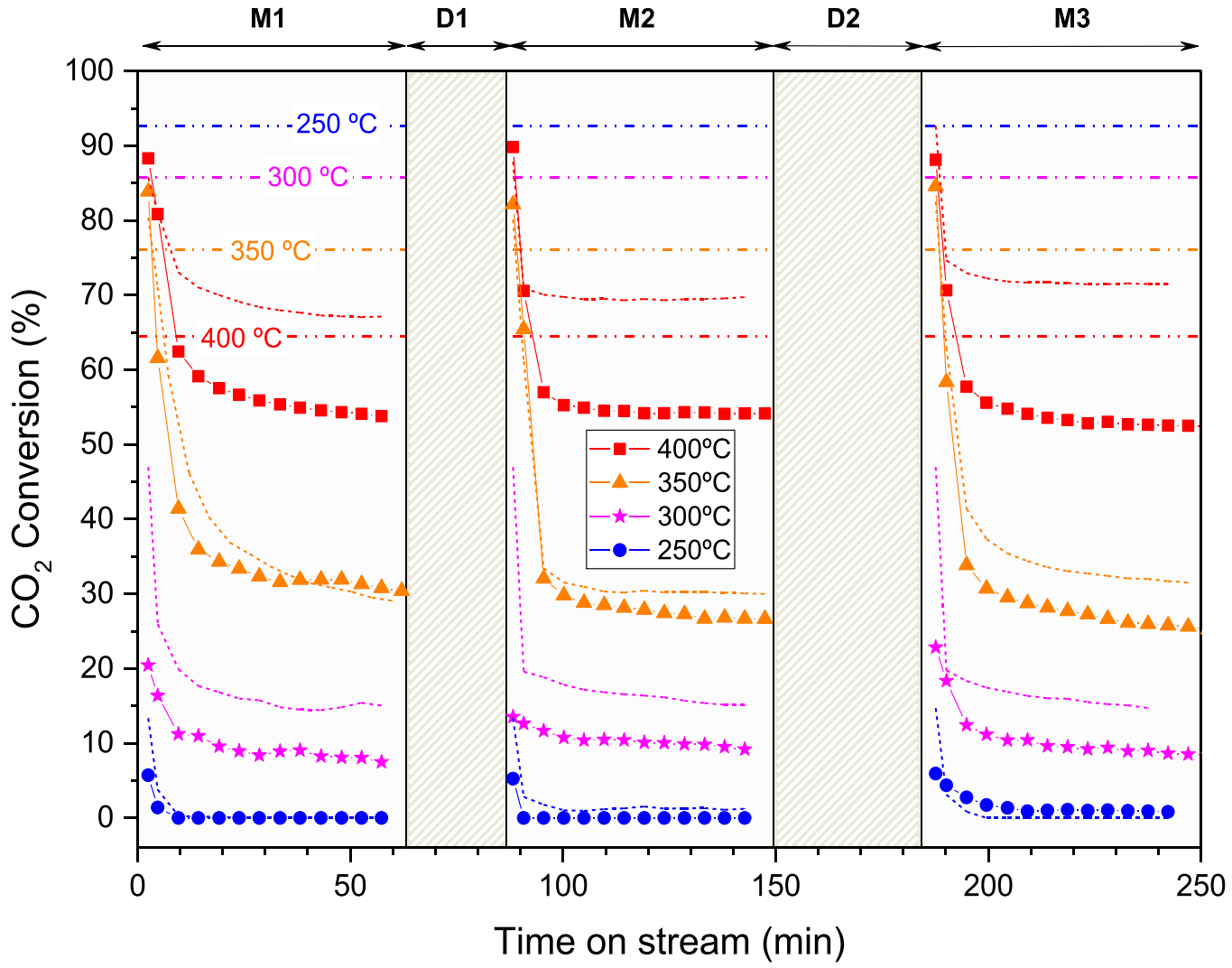

Fig. 7. CO_2 conversion for methanation-desorption experiments feeding synthetic sweetened biogas (symbols) (molar ratios H_2:CO_2:CH_4 = 12:3:7). Dotted lines correspond to experiments without presence of CH_4 in the inlet (Fig. 6) for comparison purposes. Rest of operating conditions as in Table 3. Dashed dotted lines represent equilibria conversions at different temperatures for the synthetic biogas feed. Curves between symbols only for visual guidance.

3. Results and discussion

3.1. Effect of H_2:CO_2 molar ratio of the feeding in the conversion of reactants

Inlet flow with up to five H_2:CO_2 different molar ratios (2:1, 3:1, 4:1 -stoichiometric for (r.1)-, 5:1 and 6:1), were analyzed in order to study the performance of the reactor. A comparison of H_2 and CO_2 conversions achieved vs. temperature is presented in Fig. 4 for experiments with reaction only (i.e., without adsorption by zeolite). The figure also includes the theoretical values of equilibria predicted by minimization of the *Gibbs* free energy $\left\{Min\left(\frac{\delta\Delta G}{\delta n_i}\right)\right\}$, where n_i stands for the number of atoms of the different species *-i-*, per molecule (with the aid of *Aspen HYSYS v14*).

As predictable, H_2 and CO_2 consumption showed opposite behaviors, finding higher H_2 conversions at under-stoichiometric conditions (H_2:CO_2 = 2:1 and 3:1). On the contrary, CO_2 conversion increased respecting H_2 ones for over-stoichiometric ratios (H_2:CO_2 = 5:1 and 6:1).

Results in Fig. 4 show that for all H_2:CO_2 molar ratios, equilibrium conversions decrease from lower to higher temperatures. At temperatures approaching 400 °C, experimental conversions are being limited by the thermodynamic equilibria. Note that, in order to depict this effect in Fig. 4, WHSV has been doubled respecting the "standard" value shown in Table 3 (mass of catalyst 0.5 g instead of the regular 0.25 g). The active presence of an agent capable of adsorbing water (byproduct of reactions (r.1) to (r.3)) can intensify the process, pushing up conversions even beyond the limit imposed by equilibrium, as will be shown in the next chapters.

3.2. Effect of temperature

Fig. 5 presents an experiment for 7.5Ni-2.5Fe over γ-Al_2O_3 catalyst (no Zeolite 5A present), at different temperatures with a H_2:CO_2 molar ratio of 4:1 (stoichiometric). In these experiments, the load of catalyst was half of that for experiments shown in Fig. 4 (flowrates and composition as in Table 3). That is the reason why even at 400 °C, conversions achieve lower values than those predicted by the equilibria.

The experiment began at 400 °C and ended at 250 °C. Temperature was decreased by 25 °C every ca. 50 min to allow for stabilization. The stoichiometric H_2:CO_2 ratio equal to 4:1 (*Sabatier* reaction (r.1)), showed as it was expected, identical conversions for H_2 and CO_2. As it can be observed in Fig. 5, higher temperatures improve the reactants conversion, while on the other side, equilibrium conversions (dashed lines) decrease gradually when temperature growths (right to left). No

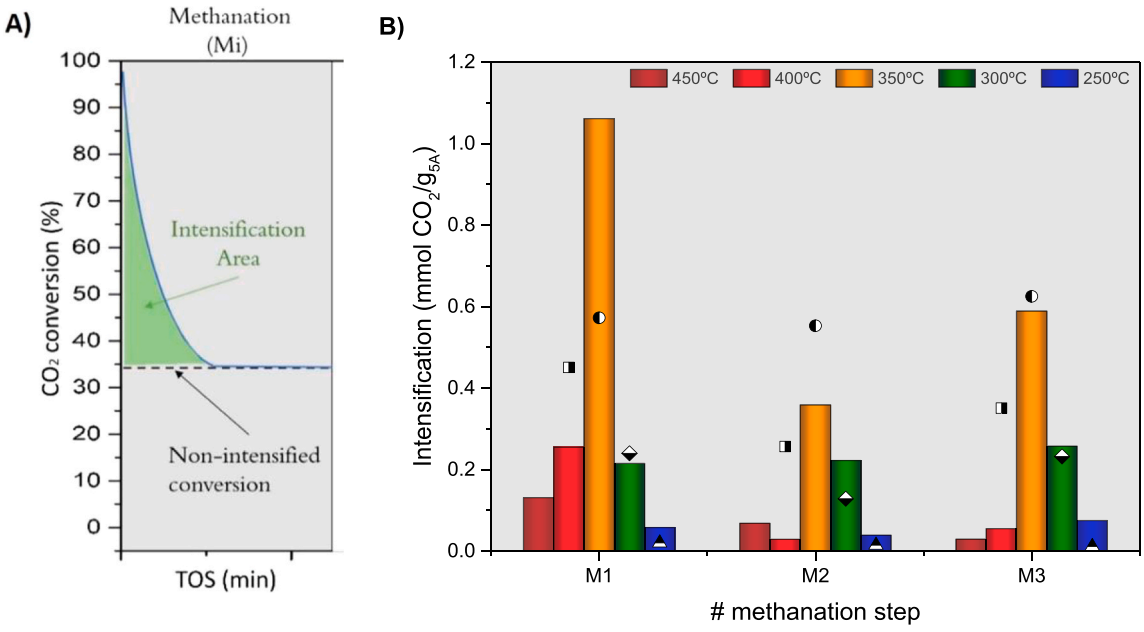

Fig. 8. A) Qualitative description of the method for determination of intensification area. B) Intensification, as mmol of CO_2 reacted in excess /g of zeolite 5A, for each temperature and methanation step (M1, M2 and M3). Bars: CO_2 methanation experiments; Symbols: Biogas methanation experiments.

significant presence of any other species (e.g., CO) was observed.

3.3. *Intensification: conversion results*

Two sets of experiments were designed to assess the positive effect of including LTA zeolite 5A in the bed to enhance the methanation reaction:

a. Hydrogenation of a CO_2 stream free of methane in the inlet.
b. Synthetic sweetened biogas upgrading (hydrogenation of CO_2 present in biogas, i.e., with CH_4 in the inlet).

3.3.1. *CO_2 methanation*

First set of enhanced methanation results (i.e., with zeolites adsorbing water from the environment), are shown in Fig. 6. Each experiment is composed by three methanation steps (labelled as M1, M2 and M3), interspersed with two desorption stages (labelled as, D1: inert atmosphere, same reaction temperature; D2: inert atmosphere, rise of temperature up to 500 °C at a rate of 5 °C /min, followed by cooling down to reaction temperature). No CH_4 was fed to the reactor for this set of experiments. Chosen stoichiometric molar ratio H_2:CO_2 was always 4:1.

As it can be observed, at all temperatures and in all methanation stages (M1, M2 and M3), CO_2 conversions reach noticeably higher values for the first few minutes of the methanation step than in the following. That behavior agrees well with the phenomenon of water adsorption by the zeolite: the removal of water from the reaction media increases the rate at with CO_2 is transformed into CH_4. Later, CO_2 conversion decreases until achieving a stationary value that is related with a non-intensified methanation regime caused by the saturation of the zeolite with water at a given temperature and steam partial pressure, given by the concurring reactions ((r.1) to (r.3)).

Also remarkable is the point that for some temperatures (400 and 450 °C), and as predicted, the values of CO_2 conversion in the early stages of the reaction, and for all methanation periods M1 through M3, are above the limit imposed by thermodynamics as consequence of H_2O retention from the reaction media by the LTA 5A.

Keeping this hypothesis in mind, a desorption period (D1) was maintained for ca. 30 min in which only inert gases were fed to the reactor keeping temperature constant. The aim was desorbing as much water from the zeolite surface as possible. After that, in the subsequent methanation (M2), with same features than (M1), the enhanced behavior decreased likewise due to the loss of the water retention capacity of the zeolite. Although initial values are comparable between M1 and M2 for a given temperature, the periods of high conversions are shorter in M2 than in M1 approaching again similar values of steady state conversions. This fact points out that the amount of water adsorbed by the zeolite has been reduced after the first methanation (M1), leading to the conclusion that some water is still adsorbed on its surface at the beginning of the M2 stage.

A second desorption (D2) was carried out increasing the temperature up to 500 °C (and subsequent cooling down) to favor complete regeneration of the zeolite by a more thorough drying. Again, similar conversions were obtained in the first moments of the third methanation (M3), followed by a more prolonged period of stabilization than in previous methanation (M2). This showed that heating in inert atmosphere (D2) promotes that conversions were almost completely recovered approaching those for fresh zeolites. It can be clearly validated, for example, at 350 °C.

From the standpoint of the behavior respecting temperature, results show that for a given methanation stage, increasing temperature clearly increases the conversion until its maximum at 400 °C. At the highest temperature (i.e., 450 °C) the thermodynamic equilibrium strongly limits the reaction and consequently, the conversion decreases respecting lower temperatures. For this temperature, although the hydrogenation rate is higher than that at lower temperatures, also the capacity of the zeolite for adsorbing water is lower, and shorter is the period for achieving a stationary state with a conversion of CO_2 ca. 65%.

Finally, for lower temperatures, although the potential of water adsorption capacity is higher than that at higher temperatures, the rate of methanation and adsorption is lower, concluding that no significant differences can be observed from one methanation to the other.

3.3.2. *Synthetic sweetened biogas methanation*

Fig. 7 presents a comparison between the CO_2 conversion along time obtained at different temperatures when only CO_2 is fed to the reactor (short-dashed curves), and when CH_4 (symbols) is jointly cofed with

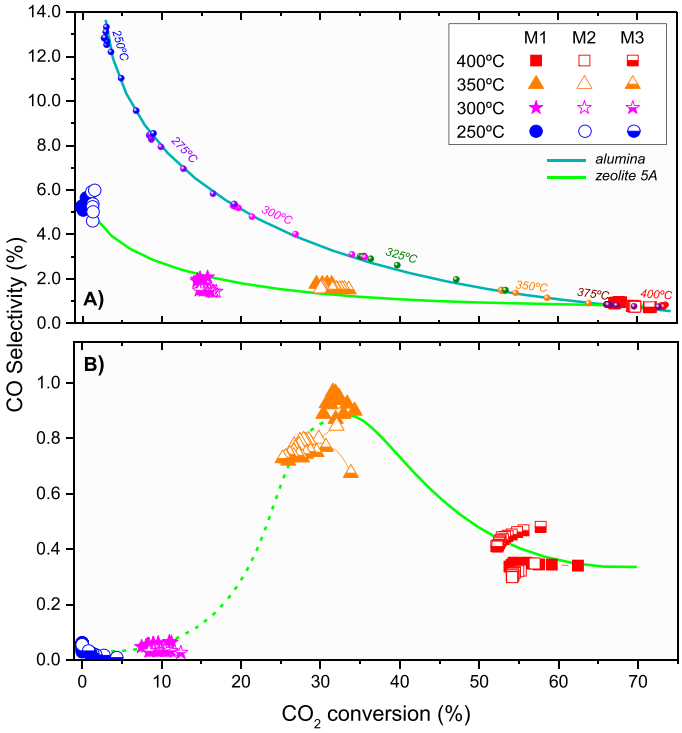

Fig. 9. Selectivity to CO vs. CO_2 conversion for different temperatures and methanation steps (M1-M3). Experimental conditions as in Table 3. Lines between data symbols only for visual guidance. A) methanation of CO_2 for both zeolite 5A and alumina as second solid in the bed. B) methanation of synthetic sweetened biogas.

CO_2. Experiments of this last type try to mimic the methanation of a biogas previously sweetened in which H_2S, siloxanes and a portion of CO_2 have been removed in an upstream cleaning process. Experimental conditions are described in Table 3.

The experiments followed the same pattern than those described in Fig. 6, with methanation steps (M1, M2 and M3) at the same temperature, interspersed by desorption stages (D1 and D2) with same temperature (D1) and previous heating up to 500 °C followed by cooling down for ensuring a thorough desorption of water (D2).

As it was seen in Fig. 6, first minutes of each methanation show values of CO_2 conversion that gradually decrease up to a point in which they remain almost stable. As described above, this behaviour can be attributed to the pushing effect of water retention by zeolite which is being saturated progressively up to a point in which zeolite can adsorb no more water. Although initial values are quite similar regardless of the presence of CH_4 in the feed or not, conversion for experiments feeding synthetic sweetened biogas show, in general, lower stationary CO_2 conversions at all temperatures. This can be explained in the light of the lower partial pressures of CO_2 entering the reactor when biogas is fed, and consequently with lower methanation rates.

The effect of sharp reduction of water adsorption capacity is also present in the event of biogas feeding. When only inert gas is passed through the bed, keeping the same temperature (D1) the amount of water released from the zeolite is lower than that adsorbed during the first methanation (M1). This capacity is almost completely recovered when desorption stage includes not only the inertization but an increase in temperature up to 500 °C and subsequent cooling down to the reaction temperature (D2).

3.4. Intensification: quantification

The method for quantifying the effect produced by introduction of zeolites in the bed in the methanation reaction, is qualitatively presented in the Fig. 8**.A**. The area below the curve describing the fall of CO_2 conversion along time achieving a stable CO_2 conversion (dashed horizontal line), represents the "extra" amount of CO_2 that has been converted into CH_4 respecting that had been converted without the aid of zeolite. This "extra" amount of CO_2, measured in (mmol/g_{LTA_5A}), can be considered an indicator of the intensification provided by the zeolite.

Mathematically, the intensification indicator (I) has been described as (Eq.1).

$$I = \frac{f^{IN}_{CO_2}}{W_{LTA5A}} \cdot \int_0^t X_{CO_2}(t) \cdot dt \tag{1}$$

where:

$f^{IN}_{CO_2}$ is the molar flow of CO_2 entering the reactor [mmol $CO_2 \cdot s^{-1}$]

X_{CO_2} is the conversion of CO_2 at the exit of the reactor as a function of time [adim]

t is the time at which CO_2 conversion has achieved a stable value [s]

W_{LTA5A} is the mass of zeolite LTA 5A present in the bed [g_{5A}]

Results shown in Fig. 6 (CO_2 methanation) and Fig. 7 (biogas methanation), were used to calculate the intensification indicator according to the inlet flow and composition to the reactor. They are presented in Fig. 8B. It can be appreciated the reduction of the zeolite capacity for adsorbing water after the first methanation-desorption cycle (from M1 to M2). However, increasing the desorption temperature along D2 (i.e., between M2 and M3), showed positive effects in the regeneration of the zeolite capacity to adsorb water. Based on these results, the optimal operation temperature for the enhanced methanation at stoichiometric H_2:CO_2 feeding rate, and rest of experimental operating conditions (as in Table 3), seems to be 350 °C. Although with significant lower values, the same trend was shown for the biogas upgrading, obtaining the highest intensification rates at the same temperature (350 °C).

3.5. Intensification: selectivity results

In some experiments, CO was found in small proportions in the exhaust gases. This is generated by the secondary non-desired reverse *Water Gas Shift* reaction (r.2), which reduces CO_2 in a parallel way to the *Sabatier* reaction (r.1), and it is favored by low temperatures due its

Table 4
Methane space-time yields (STY).

T (°C)	CH_4 STY ($mmol_{CH4}·g_{cat}^{-1}·h^{-1}$)				
	CO_2 methanation			Biogas methanation	
	WHSV = 9.7[§] $g_{CO2}·g_{cat}^{-1}·h^{-1}$	WHSV = 19.4[†] $g_{CO2}·g_{cat}^{-1}·h^{-1}$		WHSV = 13.3[‡] $g_{CO2}·g_{cat}^{-1}·h^{-1}$	
	stationary		LTA 5A intensified	stationary	LTA 5A intensified
400	175.9	293.3	306.6	162.0	181.6
350	156.7	128.4	173.9	89.6	131.8
300	71.6	65.0	78.9	22.6	42.4
250	13.4	4.2	14.1	1.5	6.6

[§] catalyst load = 0.5 g (Fig. 4) [†] catalyst load = 0.25 g (Figs. 6, 8, and 9A) [‡] catalyst load = 0.25 g (Figs. 7, 8, and 9B)

endothermic character ($\Delta H_r^0 = 41.2 kJ·mol^{-1}$). This reaction is followed in series by the reverse *Steam Methane Reaction* (r.3), so that, when the CO_2 conversion is high, the fractional yield to the intermediate product CO drastically drops. That trend was confirmed by the analysis of the results of selectivity toward CO versus CO_2 conversion shown in Fig. 9A for the experiments of CO_2 hydrogenation (Fig. 6) and sweetened biogas hydrogenation (Fig. 7). In fact, the maximum CO production is always found at very low conversions and 250 °C. When increasing temperature above 300 °C, the selectivity to CO is around three times lower. It is also remarkable the similar trend of selectivity vs. conversion for all three methanation cycles (M1 to M3). Thus, even when the zeolite adsorption capacity is reduced (i.e., for M2 compared to M1) (Fig. 8B), the selectivity of the catalytic process remains similar.

The evolution of the selectivity to CO respecting CO_2 conversion is like that found for analogous experiments but carried out loading in the bed an inert solid without hygroscopic features (alumina) instead of zeolite. The results of these latter experiments have also been included in Fig. 9A for comparison purposes. As it can be observed, apart from the transient enhancement in methanation due to water adsorption, the effect of the zeolite leads to a global decrease in selectivity to CO at all conversions and temperatures, which is a desirable effect for the global objective of CO_2 methanation.

Fig. 9B presents the CO selectivity vs CO_2 conversion comparison of the different methanation steps for biogas upgrading experiments. The feeding included a H_2:CO_2 ratio of 4:1, and CH_4:CO_2 ratio of 7:3. As it can be observed for all the cases, the selectivity to CO remains lower than 1%. The selectivity toward CO presents a decreasing trend when the CO_2 conversions approach very low values, instead of maintaining the expected exponential increase previously observed for the methanation of CO_2 free of CH_4 content (Fig. 9A). Selectivity is close to zero for temperatures below 300 °C, even when CO_2 conversion exhibited values under 10%. This change in behavior at low conversions for biogas upgrading was also observed in our laboratory with other catalytic systems such as Ni-MnO_x [4]. Comparing Fig. 9A and Fig. 9B, the inclusion of methane has significantly reduced the selectivity to CO at all temperatures, even for the highest CO_2 conversion values.

3.6. Intensification: space-time yield (CH_4 STY)

Table 4 shows the methane space-time yield (CH_4 STY) obtained at different temperatures for both CO_2 methanation and biogas methanation. In the case of zeolite-intensified operation, the average value of CH_4 STY during the intensification period (until saturation of the LTA zeolite with water) is specified. The effect of zeolite enhancing the conversion of CO_2 represents a notable increase in this average methane production.

To appreciate the advantage of intensification by adsorption, Fig. 10 shows the CH_4 STY values achieved at 300 °C in this work, and those found in recent literature. Intensification by adsorption supposes a clear increase in CH_4 STY towards its maximum stoichiometric values, even when working at WHSV greater than 10 $g_{CO2}·g_{cat}^{-1}·h^{-1}$. Moreover, the range of CH_4 STY improvement achieved by adsorption enhancement with LTA 5A zeolite at TOS = 0 (also shown in Fig. 10, apart from the average CH_4 STY value achieved during the enhanced period) is clearly significant. The effect is remarkably greater in the case of CO_2 methanation than in the case of biogas methanation.

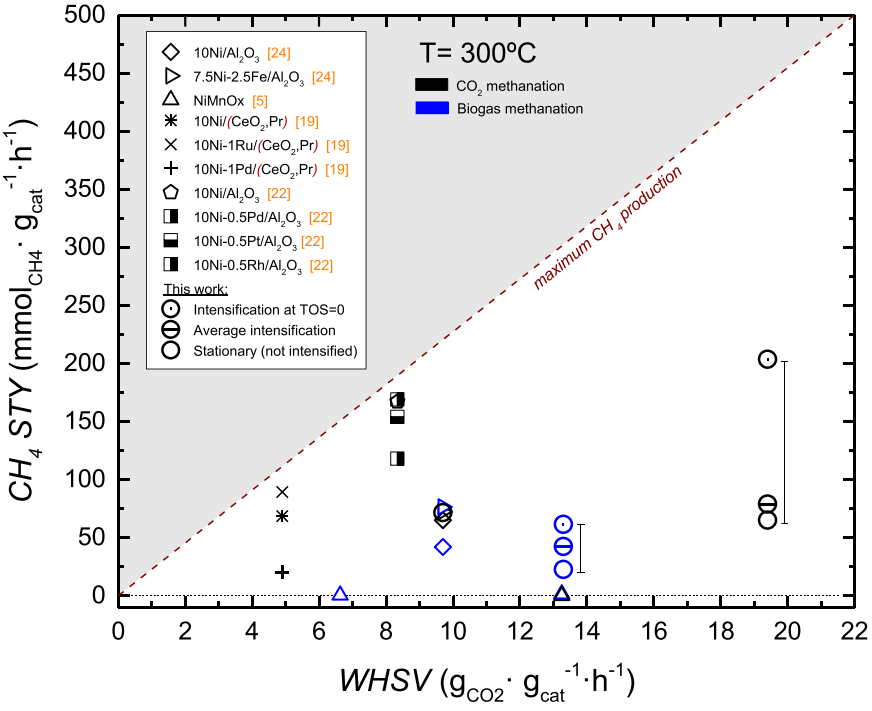

Fig. 10. Methane space-time yields (CH_4 STY) vs. WHSV for several bibliographic references at 300 °C, including those obtained in this work.

4. Conclusions

This study evidences the possibility of thermochemically increase the content of methane of a sweetened biogas by thermocatalytic hydrogenating the CO_2 present in the mixture (Sabatier reaction). The characterization of the catalysts (BET, XRF, XRD and H_2-TPR) corroborated the correct catalyst synthesis, pointing out that the specific surface of the 7.5Ni-2.5Fe catalyst over gamma-alumina remained high even though it was subjected to a prior calcination at 500 °C for a period of 8 hours.

Respecting intensification of the process, LTA 5A zeolite has proved to enhance de CO_2 hydrogenation for temperatures over 350 °C. The role of zeolite in the bed is taking water from the reacting media, pushing the catalyzed methanation reaction towards products beyond the point the catalyst would do if it were alone. In addition, for the first methanation step, CO_2 conversion increased more than 20% compared to the original (i.e., without zeolite) stationary conversion. As drawback, intensification behavior was reduced after the first methanation cycle and it only was recovered after a desorption step rising the temperature up to 500 °C.

Catalyst showed stability after the methanation plus adsorption-desorption cycles with and without CH_4 feeding. In general, inclusion of CH_4 in the feed reduces the stationary conversion behaving as a pseudo-inert species. However, at 350 °C the conversion reduction was minimal and the reduction in the intensification behavior was less pronounced, making 350 °C the optimal temperature among those checked. On the other hand, CH_4 addition in the inlet has a positive effect by decreasing the selectivity towards CO at a given CO_2 conversion for all the temperatures tested, compared to those without CH_4 present in the feed.

CRediT authorship contribution statement

Jose-Angel Peña: Writing – review & editing, Validation, Supervision, Project administration, Funding acquisition. **Paúl Durán:** Resources, Investigation. **Víctor Daniel Mercader:** Writing – original draft, Investigation, Data curation. **Eva Francés:** Supervision, Formal analysis, Conceptualization. **Pablo Aragüés-Aldea:** Visualization, Investigation. **Javier Herguido:** Writing – review & editing, Validation, Supervision, Methodology, Formal analysis, Conceptualization.

Declaration of Competing Interest

The authors declare that they have no known competing financial interests or personal relationships that could have appeared to influence the work reported in this paper.

Data Availability

Data will be made available on request.

Acknowledgements

This research was funded by MICINN (*Spanish Ministerio de Ciencia e Innovación*) projects number PID2019–104866RB-I00, PID2022–136947OB-I00 and European Union Next Generation PRTR-C17.I1 Task LA4.A1. In addition, the consolidated research group *Catalysis and Reactor Engineering Group* (CREG) (T43–23R) has the financial support of Gobierno de Aragón (*Aragón*, Spain) through the European Social Fund – FEDER. Also V.D. Mercader and P. Aragüés-Aldea want to express their gratitude for the research grants of *Ministerio de Ciencia e Innovación* (VDM) (grant no. PRE2020–095679) and *Gobierno de Aragón* (PAA) respectively. Finally, authors also would like to acknowledge the use of *Servicio General de Apoyo a la Investigación-SAI* (Universidad de Zaragoza).

References

[1] European Statistics-Eurostat, Energy, Transport and Environment Statistics 2020 edition, 2020.
[2] European Commission, State of the Energy Union Report 2023, Brussels, 2023.
[3] M.U. Alzueta, J. Giménez-López, V.D. Mercader, R. Bilbao, Conversion of NH_3 and NH_3-NO mixtures in a CO_2 atmosphere. A parametric study, Fuel 327 (2022), https://doi.org/10.1016/J.FUEL.2022.125133.
[4] H. Zhou, J. Wang, W. Meng, K. Wang, G. Li, Y. Yang, Z. Fan, D. Wang, D. Ji, Comparative investigation of CO_2-to-methanol process using different CO_2 capture technologies, Fuel 338 (2023) 127359, https://doi.org/10.1016/J.FUEL.2022.127359.
[5] P. Aragüés-Aldea, A. Sanz-Martínez, P. Durán, E. Francés, J.A. Peña, J. Herguido, Improving CO_2 methanation performance by distributed feeding in a Ni-Mn catalyst fixed bed reactor, Fuel 321 (2022) 124075, https://doi.org/10.1016/J.FUEL.2022.124075.
[6] M. Thema, F. Bauer, M. Sterner, Power-To-gas: electrolysis and methanation status review, Renew. Sustain. Energy Rev. 112 (2019) 775–787, https://doi.org/10.1016/j.rser.2019.06.030.
[7] I. Angelidaki, L. Treu, P. Tsapekos, G. Luo, S. Campanaro, H. Wenzel, P.G. Kougias, Biogas upgrading and utilization: current status and perspectives, Biotechnol. Adv. 36 (2018) 452–466, https://doi.org/10.1016/J.BIOTECHADV.2018.01.011.
[8] M. Thema, F. Bauer, M. Sterner, Power-to-gas: electrolysis and methanation status review, Renew. Sustain. Energy Rev. 112 (2019) 775–787, https://doi.org/10.1016/J.RSER.2019.06.030.
[9] S.S. Cordova, M. Gustafsson, M. Eklund, N. Svensson, What should we do with CO_2 from biogas upgrading? J. CO2 Util. 77 (2023) 102607 https://doi.org/10.1016/J.JCOU.2023.102607.
[10] M.U. Khan, J.T.E. Lee, M.A. Bashir, P.D. Dissanayake, Y.S. Ok, Y.W. Tong, M. A. Shariati, S. Wu, B.K. Ahring, Current status of biogas upgrading for direct biomethane use: a review, Renew. Sustain. Energy Rev. 149 (2021) 111343, https://doi.org/10.1016/J.RSER.2021.111343.
[11] P. Sabatier, J. Senderens, New methane synthesis, CR Acad. Sci. 134 (1902) 514–516.
[12] L. Pastor-Pérez, F. Baibars, E. Le Sache, H. Arellano-García, S. Gu, T.R. Reina, CO_2 valorisation via reverse water-gas shift reaction using advanced Cs doped Fe-Cu/Al_2O_3 catalysts, J. CO2 Util. 21 (2017) 423–428, https://doi.org/10.1016/J.JCOU.2017.08.009.
[13] A.H. Hatta, A.A. Jalil, N.S. Hassan, M.Y.S. Hamid, W. Nabgan, M. Alhassan, M. B. Bahari, C.K. Cheng, S.H. Zein, M.L. Firmansyah, A short review on informetric analysis and recent progress on contribution of ceria in Ni-based catalysts for enhanced catalytic CO methanation, Powder Technol. 417 (2023) 118246, https://doi.org/10.1016/J.POWTEC.2023.118246.
[14] K. Ghaib, F.Z. Ben-Fares, Power-to-methane: a state-of-the-art review, Renew. Sustain. Energy Rev. 81 (2018) 433–446, https://doi.org/10.1016/j.rser.2017.08.004.
[15] C. Dannesboe, J.B. Hansen, I. Johannsen, Catalytic methanation of CO_2 in biogas: experimental results from a reactor at full scale, React. Chem. Eng. 5 (2019) 183–189, https://doi.org/10.1039/C9RE00351G.
[16] C.H. Tan, S. Nomanbhay, A.H. Shamsuddin, Y.K. Park, H. Hernández-Cocoletzi, P. L. Show, Current developments in catalytic methanation of carbon dioxide—a review, Front. Energy Res. 9 (2022), https://doi.org/10.3389/fenrg.2021.795423.
[17] N.D.M. Ridzuan, M.S. Shaharun, M.A. Anawar, I. Ud-Din, Ni-based catalyst for carbon dioxide methanation: a review on performance and progress, Page 469 12, Catalysts Vol. 12 (2022) 469, https://doi.org/10.3390/CATAL12050469.
[18] A.I. Tsiotsias, N.D. Charisiou, I.V. Yentekakis, M.A. Goula, Bimetallic Ni-based catalysts for CO_2 methanation: a review, Nanomaterials Vol. 11 (2020) 28, https://doi.org/10.3390/NANO11010028. Page 28 11.
[19] A.I. Tsiotsias, N.D. Charisiou, C. Italiano, G.D. Ferrante, L. Pino, A. Vita, V. Sebastian, S.J. Hinder, M.A. Baker, A. Sharan, N. Singh, K. Polychronopoulou, M.A. Goula, Ni-noble metal bimetallic catalysts for improved low temperature CO_2 methanation, Appl. Surf. Sci. 646 (2024) 158945, https://doi.org/10.1016/J.APSUSC.2023.158945.
[20] A.I. Tsiotsias, N.D. Charisiou, E. Harkou, S. Hafeez, G. Manos, A. Constantinou, A. G.S. Hussien, A.A. Dabbawala, V. Sebastian, S.J. Hinder, M.A. Baker, K. Polychronopoulou, M.A. Goula, Enhancing CO_2 methanation over Ni catalysts supported on sol-gel derived Pr_2O_3-CeO_2: an experimental and theoretical investigation, Appl. Catal. B 318 (2022) 121836, https://doi.org/10.1016/J.APCATB.2022.121836.
[21] A.I. Tsiotsias, N.D. Charisiou, A. AlKhoori, S. Gaber, V. Stolojan, V. Sebastian, B. van der Linden, A. Bansode, S.J. Hinder, M.A. Baker, K. Polychronopoulou, M. A. Goula, Optimizing the oxide support composition in Pr-doped CeO_2 towards highly active and selective Ni-based CO_2 methanation catalysts, J. Energy Chem. 71 (2022) 547–561, https://doi.org/10.1016/J.JECHEM.2022.04.003.
[22] M. Mihet, M.D. Lazar, Methanation of CO_2 on Ni/γ-Al_2O_3: Influence of Pt, Pd or Rh promotion, Catal. Today 306 (2018) 294–299, https://doi.org/10.1016/J.CATTOD.2016.12.001.
[23] D. Pandey, G. Deo, Effect of support on the catalytic activity of supported Ni–Fe catalysts for the CO_2 methanation reaction, J. Ind. Eng. Chem. 33 (2016) 99–107, https://doi.org/10.1016/J.JIEC.2015.09.019.
[24] A. Sanz-Martínez, P. Durán, V.D. Mercader, E. Francés, J.Á. Peña, J. Herguido, Biogas upgrading by CO_2 methanation with Ni-, Ni-Fe-, and Ru-based catalysts, Catalysts 12 (2022), https://doi.org/10.3390/catal12121609.